NANO LETTERS

2007
Vol. 7, No. 8
2188−2195

Vertically Aligned Carbon Nanofiber Arrays Record Electrophysiological Signals from Hippocampal Slices

Zhe Yu,[†] Timothy E. McKnight,[‡,§] M. Nance Ericson,[§] Anatoli V. Melechko,[‡,||] Michael L. Simpson,[‡,||] and Barclay Morrison III*,[†]

Department of Biomedical Engineering, Columbia University, 1210 Amsterdam Avenue, 351 Engineering Terrace, New York, New York 10027, and Molecular Scale Engineering and Nanoscale Technologies Research Group, Monolithic Systems Development Group, and Center for Nanophase Material Science, Oak Ridge National Laboratory, P.O. Box 2008, Oak Ridge, Tennessee 37831

Received February 5, 2007; Revised Manuscript Received May 25, 2007

ABSTRACT

Vertically aligned carbon nanofiber (VACNF) electrode arrays were tested for their potential application in recording neuro-electrophysiological activity. We report, for the first time, stimulation and extracellular recording of spontaneous and evoked neuroelectrical activity in organotypic hippocampal slice cultures with ultramicroelectrode VACNF arrays. Because the electrodes are carbon-based, these arrays have potential advantages over metal electrodes and could enable a variety of future applications as precise, informative, and biocompatible neural interfaces.

Technological developments have driven wider adoption of microelectrode array (MEA) based studies which are capable of recording activity from multiple neurons simultaneously, thereby increasing our understanding of neuronal network physiology (see for review refs 1 and 2). Herein we report the development of a new MEA consisting of vertically aligned carbon nanofibers (VACNFs) and demonstrate its ability to stimulate and record from organotypic hippocampal brain slice cultures, recapitulating the functionality of contemporary MEAs. The nanometer dimension and versatility of carbon nanofibers coupled to a high-density MEA layout could enable future studies not possible with metal-based MEAs or carbon fiber electrodes.

The first extracellular MEA recordings were reported from contracting myocyte sheets.[3] The arrays were constructed on glass from wet-etched, vacuum-deposited nickel. The nickel was gold plated and insulated with a polymer, and the exposed electrodes were plated with platinum black.[3−6] Invertebrate neuronal action potentials were first recorded with an MEA of similar construction (titanium and gold conductors) with smaller electrodes exposed by laser ablation of the insulation.[7,8] The first MEA recordings from dissociated mammalian superior cervical ganglia neurons were made shortly thereafter with platinized chromium and gold conductors insulated with silicon dioxide[9] followed by recordings from dissociated spinal-cord neurons from titanium and gold conductors insulated with a hydrophobic polysiloxane layer.[10] Alternatively, polyimide was also used as an insulation layer in these early MEAs[11] to first record from hippocampal slices.[12,13] MEAs of transparent indium tin oxide conductors were first reported in 1985.[14] It is biocompatible,[14] and low noise recording and stimulation can be achieved by gold plating or platinizing.[15,16]

Technological advancements continue to increase the number of applications for MEAs and improve their functionality. Specialized MEA designs include perforated arrays for long-term organotypic brain slice culturing[17,18] and arrays with custom electrode geometries to match neuroanatomical structures.[19] MEAs have also been designed to interrogate neural function at the single cell level with electrodes surrounded by microcages for spatially confining neurons or at the subcellular level[20] with electrodes as small as 2 μm[21] or even fabricated from silicon nanowires.[22]

Planar MEAs have electrodes confined to the substrate plane and cannot penetrate into tissues. The surface of acutely sectioned tissue slices is comprised of injured or dead cells, and the surface of slice cultures may consist of a reactive glia layer; both reduce signal propagation from the active cells to the electrodes.[23] To improve signal quality, two groups have designed and tested MEAs with three-dimen-

* Corresponding author: tel, 212-854-6277; fax, 212-854-8725; e-mail, bm119@columbia.edu.
[†] Department of Biomedical Engineering, Columbia University.
[‡] Molecular Scale Engineering and Nanoscale Technologies Research Group, ORNL.
[§] Monolithic Systems Development Group, ORNL.
[||] Center for Nanophase Material Science, ORNL.

10.1021/nl070291a CCC: $37.00
Published on Web 06/30/2007

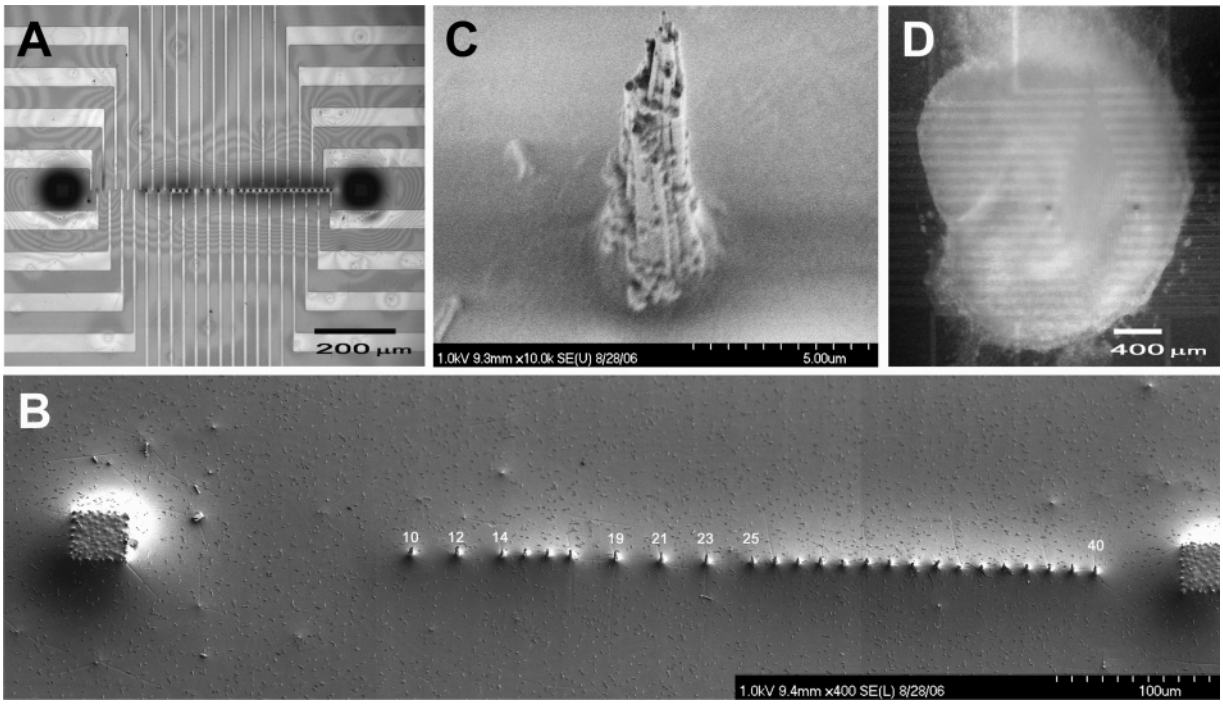

Figure 1. Images of VACNF arrays: (A) Light micrograph of a VACNF array before use. Notice that electrodes 1−9, 11, 13, 18, 20, 22, and 24 are not present due to absence of catalyst prior to fiber growth at these locations. (B) SEM image of the entire VACNF array from (A) acquired after several electrophysiological recordings. The missing electrodes were not sheared off during use as indicated by the smooth layer of SU-8 where they should be. (C) An SEM image of a VACNF electrode from the same array in (B). The SEM images indicate that the VACNF electrodes are mechanically robust and are not sheared by the process of multiple recordings. (D) Light micrograph of a hippocampal slice (22 DIV) on the VACNF array chip. Hippocampal slices were cultured separately and then transferred to precoated arrays.

sional (3-D) electrodes to penetrate into the tissue.[17,18,24,25] The Ayanda Biosystems arrays[24,26] and the other[27−29] employ pyramidal platinum electrodes approximately 50 μm tall for recording and stimulation.

Carbon nanofibers (CNFs) are finding a growing number of novel applications, particularly in the biological arena because of their inherent biocompatibility and stability in physiological solutions.[30−33] Recent advances in CNF synthesis have produced VACNF arrays which are high aspect ratio, deterministically synthesized nanostructures[34−47] which we have previously integrated with conventional microelectronics either in planar geometries or in flexible polymer membranes.[48] Recently, we have made progress in producing VACNFs with controlled geometries and lengths in excess of 10 μm.[49] The synthesis process is compatible with microfabrication techniques which provide advantages of parallel fabrication at high densities (down to 2 μm pitch) with high spatial resolution.[44] VACNF arrays have been mated to substrate embedded conductors to produce multiscale MEA chips for electrochemical sensing applications[45,50] but have not recorded electrical activity in neural tissue. Here we report for the first time the critical accomplishment of stimulating and recording from neural tissue with a VACNF MEA.

Methods and Results. The fabrication of VACNF arrays has been reported in detail previously.[46,47,50] Briefly, to fabricate VACNF arrays, n-type silicon wafers are insulated with 1 μm of silicon dioxide followed by metallization with 100 Å of Ti, 1000 Å of W, 100 Å of Ti, and 100 Å of Si using electron-beam evaporation in vacuum at base pressure lower than 10^{-6} Torr. 1000 Å thick Ni catalyst dots of 2 μm diameter at 15 μm spacing were defined lithographically for fiber growth. At each dot, groups of vertically aligned carbon nanofibers were grown 10 μm tall by direct current catalytic plasma enhanced chemical vapor deposition (dc C-PECVD) by tip-type fiber growth. Interconnects were defined by contact photolithography, and realized by reactive ion refractory metal etch ($SF_6/O_2/CHF_3$). A conformal passivation layer of silicon dioxide (~1000 Å thick) was deposited by PECVD followed by a 3−5 μm thick spun layer of SU-8 to further passivate the substrate interconnects which was then removed from the contact pads and electrode tips. A subsequent HF buffered oxide etch removed the exposed silicon oxide coating from nanofibers above the SU-8 layer and from the substrate interconnects. Individual VACNF array chips were then diced, packaged, and autoclaved (121 °C, 20 min) for sterilization before use.

The arrays used for this study were type II architectures[50] which consisted of a linear array of 40, individually addressed VACNF electrodes, 10 μm in height, spaced 15 μm apart along a total length of 600 μm as shown under light (Figure 1A) or scanning electron microscopy (Figure 1B). Discrete nanofiber electrodes were inspected following hippocampal culture and recording with a Hitachi 4700S scanning electron microscope. Parts B and C of Figure 1 were acquired after the array was used for recording from multiple slice cultures, indicating that the VACNF electrodes are mechanically robust and were not sheared during tissue positioning and removal. For the particular chip shown in this figure, terminal

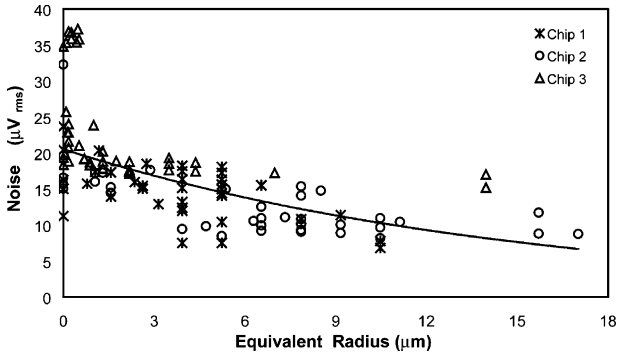

Figure 2. Root-mean-squared noise levels were recorded for each electrode of three separate VACNF array chips in an aCSF solution in the absence of tissue. Noise was plotted as a function of effective electrode size as determined from the steady-state reduction current in 1 mM ruthenium hexamine trichloride (119 electrodes total). The exponential trend line indicates that the noise level decreases with increasing VACNF electrode size.

fibers at electrodes 1−9, 11, 13, 18, 20, 22, and 24 were not present before recording due to absence of the catalyst particle at these locations prior to fiber growth (Figure 1A). These fibers were not sheared off during recording as evidenced by the smooth SU-8 surface and lack of a VACNF stub. This mechanical resilience of nanofibers is consistent with other studies where nanofiber arrays remain intact after mechanical interaction with tissue for gene delivery applications.[51] Individual VACNF electrodes were conelike in shape (Figure 1C) allowing the electrodes to penetrate into the tissue to improve electrical coupling. To record electrical activity, a hippocampal slice was positioned on the VACNF array and oriented with respect to the anatomy (Figure 1D). After the electrical activity was recorded, the tissue was gently removed before another culture was positioned on the VACNF array.

The VACNF electrodes are smaller than traditional MEA electrodes; therefore the effect of electrode size on electrode $\text{noise}_{\text{rms}}$ was determined. The steady-state reduction current of 1 mM ruthenium hexamine trichloride in 300 mM KCl was determined from cyclic voltammetric sweeps from +100 to −600 mV against a Ag|AgCl (3 M KCl) reference electrode in two-wire mode.[47,50] Steady-state current at −250 mV was converted to radius by assuming a semihemispherical electrode shape and employing the relationship

$$\text{radius} = \frac{i_{\text{ss}}}{2\pi nFDC} \tag{1}$$

where i_{ss} is the steady-state reduction current, n is the number of electrons transferred during the reduction (i.e., 1), F is Faraday's constant, D is the diffusion coefficient of $Ru(NH_3)_6^{3+}$ ($D = 6.3 \times 10^{-6}$ cm^2/s), and C is the concentration of the analyte (i.e., 0.001 M). As shown in Figure 2A, the equivalent radius of most electrodes was less than 10 μm (119 electrodes from 3 chips, 4.02 μm average). The average noise level was 17 μV_{rms} and was dependent on electrode dimension, with larger electrodes producing less noise. The noise on most electrodes, including the majority of the smallest was below 25 μV_{rms} enabling extracellular electrophysiological recordings from organotypic hippocampal slice cultures. These noise levels compare favorably to other MEA electrodes: indium tin oxide (30−40 μV), platinum (20−25 μV), titanium nitride (10−25 μV), platinum black (5−10 μV), and the Ayanda 3-D arrays (14−17 μV).[25]

The long-term culture of hippocampal tissue slices has been described in detail previously.[52] All animal procedures were approved by the Columbia University IACUC. The hippocampus of a postnatal day 8−11 rat pup was removed aseptically and cut into sections 400 μm thick with a McIlwain tissue chopper (Mickle Laboratory Engineering Co., U.K.). Slices were transferred to Millicell-CM membranes (Millipore) in six-well culture plates (Fisher) and fed through the membrane with nutrient medium (50% minimum essential medium with Earle's salts, 25% heat inactivated horse serum, 25% Hank's balanced salt solution, 1 mM glutamine, and 4.5% glucose, Invitrogen).[53] Cultures were maintained in an incubator (5% CO_2, 37 °C) for 2−3 weeks before use.

Carbon fibers have been used previously to record electrophysiology in slice culture, but never in a high density, microfabricated format. Prior to recording, VACNF chips were cleaned by air plasma treatment (Harrick PDC-32G, Harrick Scientific Corp.) for 30 s, and then coated with a mixture of poly-L-lysine (320 μg/mL, Sigma) and laminin (80 μg/mL, Invitrogen) in water overnight followed by three washes with water. The arrays were inserted into the multichannel amplifier (MEA1060-Inv-BC, MultiChannel Systems, Germany) which maintained the temperature at 37 °C throughout the duration of the recording. Individual cultures were cut from their membranes and inverted onto VACNF arrays in artificial cerebrospinal fluid (aCSF in mM: 125 NaCl, 3.5 KCl, 26 $NaHCO_3$, 1.2 KH_2PO_4, 1.3 $MgCl_2 \cdot 6H_2O$, 2.4 $CaCl_2$, 10 glucose; pH = 7.40). A nylon mesh was used to hold tissue in place during perfusion and measurement. Signals were sampled at 20 kHz with a 5 kHz analog, antialiasing filter.

Spontaneous electrical activity of hippocampal slices was recorded with the VACNF array chips (Figure 3). Tissue was aligned with the electrode array crossing the hilus of the hippocampus (Figure 3A) with electrode 1 located in the CA3 pyramidal cell layer and electrode 40 in the dentate gyrus (DG) granule cell layer (Figure 3B). Spontaneous complex spikes were recorded on multiple electrodes placed in the CA3 pyramidal cell layer (electrodes around 1) and granule cell layer (electrodes around 40). Figure 3C shows complex spikes recorded from the granule cell layer (electrode 38). The spontaneous complex spikes (amplitude of ~50 μV_{pp}) were readily detected above the background noise of about 25 μV_{rms}. The spontaneous activity was blocked by 1 μM tetrodotoxin (TTX, Sigma, inset Figure 3C), a voltage-sensitive sodium channel blocker, which reduced the firing rate to zero within 3 min after introduction (Figure 3D). Complex spike firing rate was calculated by binning time in windows of 10 s and counting spikes. These results indicate that the spontaneous activity recorded by the VACNF array chips was of biological origin and not electrical interference.

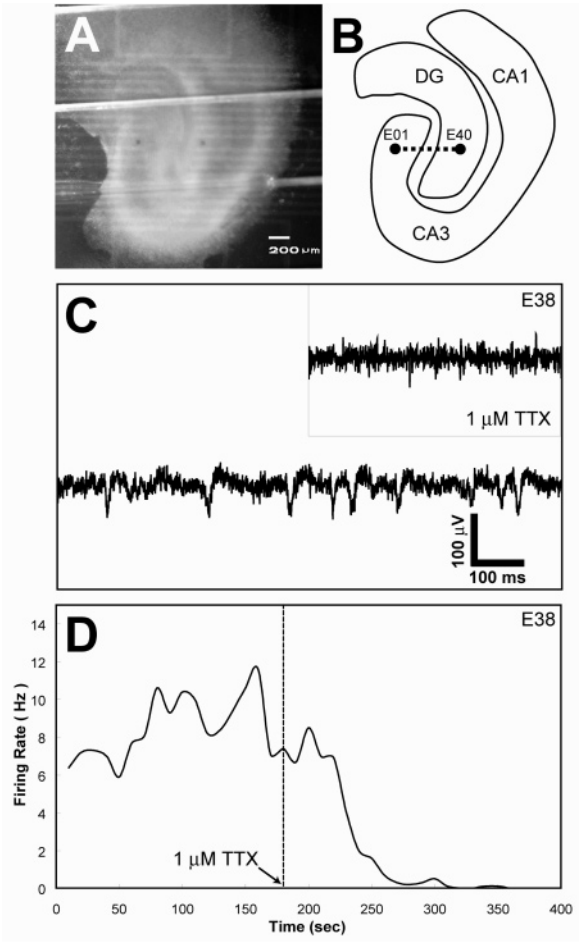

Figure 3. The VACNF arrays were capable of recording spontaneous activity in hippocampal slices. (A) Light micrograph of a hippocampal slice (13 DIV) on a VACNF array chip. A nylon mesh, which is typically used for MEA recording to secure the tissue, is evident. (B) A schematic of the hippocampus anatomy depicts the electrode recording locations which crossed the hilus region from the CA3 pyramidal layer to the DG granule cell layer. (C) Spontaneous activity demonstrating complex spikes recorded from one channel is depicted (electrode 38). The amplitude of spikes ranged from 30 μV to more than 60 μV. The spontaneous complex spikes were diminished by 1 μM TTX (inset), indicating the signals were of biological origin. (D) Firing rate decreased to zero after administration of 1 μM TTX.

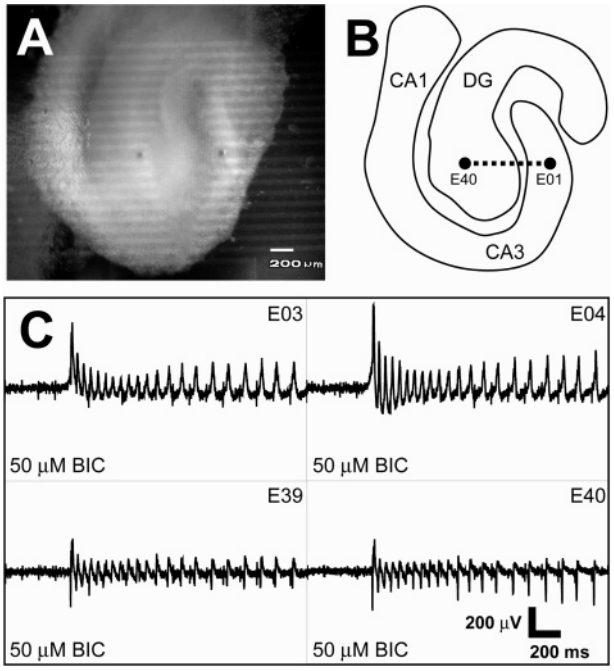

Figure 4. Bicuculline-induced epileptiform activity was recorded from hippocampal slices with the VACNF array chips. (A) A light micrograph of a hippocampal slice (13 DIV) on a VACNF array chip. (B) A schematic of the hippocampal anatomy depicts the electrode recording locations. The electrode array crossed the hilus region from the DG granule cell layer to the CA3 pyramidal layer. (C) BIC-induced epileptiform activity as shown for four channels (electrodes 3, 4, 39, and 40). Compared to the spontaneous activity shown in Figure 3, BIC induced continuous large oscillations with amplitudes up to 600 μV.

Inhibitory neuronal circuits within the hippocampus restrict spontaneous activity under normal conditions with the majority of inhibition mediated by the $GABA_A$ receptor, which can be blocked by (−)-bicuculline methiodide (BIC, Sigma). Administration of 50 μM BIC induced spontaneous epileptiform activity which was recorded with the VACNF array chips (Figure 4). A hippocampal slice was placed on an array crossing the hilus region (Figure 4A) with electrode 1 in the DG granule cell layer and electrode 40 in the CA3 pyramidal cell layer (Figure 4B). BIC-induced epileptiform activity propagated throughout the hippocampal slice and was detected on multiple channels (Figure 4C). In contrast to spontaneous activity, the BIC-induced epileptiform activity consisted of large oscillations with amplitudes 10 times greater than spontaneous complex spikes.

Evoked responses were recorded (Figure 5 and Figure 6) in response to constant current, bipolar stimuli applied between two VACNF electrodes using a MultiChannel Systems programmable stimulator (STG1004, MultiChannel Systems, Germany). The stimulus waveform was constant current, biphasic: positive first for 100 μs followed by a negative phase for 100 μs. A sync pulse for 300 μs, covering each 200 μs stimulus, was simultaneously generated by the stimulator to provide a stimulus trigger for the recording system. As shown in Figure 5A, a hippocampal slice was placed on an electrode array with electrode 1 in the DG granule cell layer and electrode 40 in the CA3 pyramidal cell layer. A constant current, bipolar, biphasic stimulus (50 μA) was applied across electrodes 2 and 3, located within the DG granule cell layer (Figure 5B). As shown in Figure 5C, the evoked field potential recorded in the hilus (electrode 20) was different from that in the CA3 pyramidal cell layer (electrode 40). To differentiate evoked field potentials from stimulus artifacts, a cocktail of 1 μM TTX, 50 μM BIC, 100 μM *d*-2-amino-5-phosphonovaleric acid (APV, NMDA receptor antagonist; Sigma), and 100 μM 6-cyano-7-nitroquinoxaline-2,3-dione disodium salt (CNQX, non-NMDA glutamate receptor antagonist; TOCRIS) was introduced to block synaptic transmission and spontaneous activity. In the presence of these compounds, the evoked field potentials were blocked both in the cell layers and in the hilus, with the remaining signal attributable to stimulation artifact (Figure 5D). The artifact was generated, in part, by the stimulator sync pulses and was present when the stimulus intensity was set to zero. The stimulus artifact could be

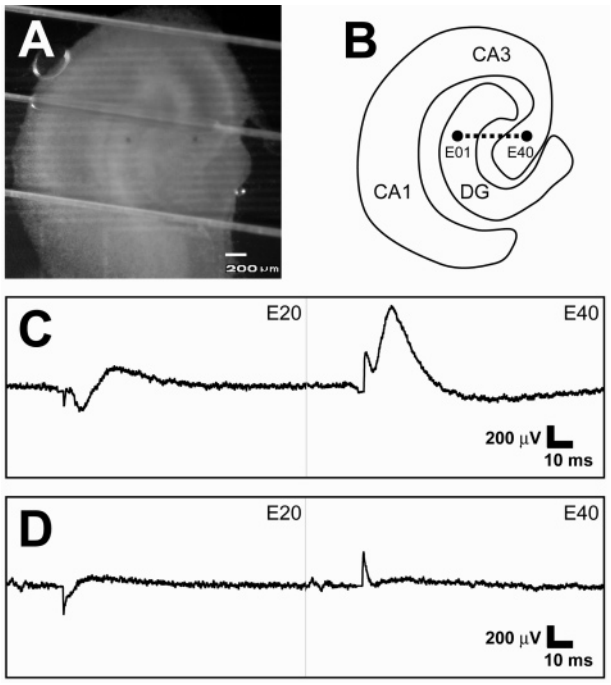

Figure 5. Evoked field potentials were recorded from hippocampal slices by the VACNF array chips. (A) Light micrograph of a hippocampal slice (13 DIV) on a VACNF chip with the nylon mesh evident. (B) A schematic of the hippocampal anatomy depicting the recording locations which crossed the hilus region from the DG granule cell layer to the CA3 pyramidal layer. (C) Evoked field potentials recorded from two channels (electrodes 20 and 40) are shown, which were elicited by a constant current, bipolar, biphasic stimulus of 50 μA applied to electrodes 2 and 3. The trace from electrode 20 shows a typical evoked field potential recorded from the dendritic layer, whereas the trace from electrode 40 shows a typical evoked field potential recorded from the pyramidal cell body layer. (D) The evoked field potentials were eliminated with a pharmacological cocktail of neuronal channel and receptor antagonists (1 μM TTX, 50 μM BIC, 100 μM APV, and 100 μM CNQX). The remaining signal was a stimulus artifact.

further differentiated from evoked responses because of its short latency of less than 5 ms. The evoked presynaptic potential has a minimum latency of about 1 ms whereas the evoked postsynaptic potential has a latency of 3−5 ms resulting in little overlap of the latter with the stimulus artifact.

The ability of the VACNF array chips to measure evoked field potentials was further investigated (Figure 6). A hippocampal slice was aligned to a VACNF chip with electrode 1 in the DG granule cell layer and electrode 40 in the CA3 pyramidal cell layer. A constant current, bipolar biphasic stimulus was applied to electrodes 11 and 29 located within the DG granule cell layer and the CA3 stratum radiatum, respectively (parts A and B of Figure 6). The amplitude and slope of evoked field potentials recorded from the CA3 pyramidal cell layer were calculated as shown in Figure 6C. From evoked responses, stimulus/response (*S*/*R*) curves were constructed by increasing the intensity of a biphasic, bipolar stimulus in 10 μA increments from 10 to 100 μA and recording the corresponding response at other electrodes. The mean and standard deviation were calculated from three trials. For a given channel, the response magnitude was plotted against the stimulus magnitude and fit to a sigmoidal function of the form

$$R(S) = R_0 + \frac{R_{\max}}{1 + e^{m(I_{50} - S)}} \tag{2}$$

where R is the evoked response, R_0 is the background response, $R_{\max}$ is the maximum response, I_{50} is the current which produces a half-maximal response, S is the intensity of stimulus, and m is proportional to the slope of the linear region of the sigmoid.

Although the background R_0 was not zero due to the sync pulse artifact, it was stable for all three channels ($\sim$150 μV). As the *S*/*R* curves (parts D and E of Figure 6) show, the amplitude and slope increased as the stimulus intensity increased as more neurons were stimulated. The maximal value of the *S*/*R* curve corresponds to the total number of neurons excited by the stimulation. Therefore, the recorded response decreased as a function of distance from the stimulation site with electrode 32 being proximal (higher response) and electrode 40 distal (lower response). However, I_{50}, the current of half-maximal stimulation which is related to excitability, was unchanged due to similarity of the pyramidal neurons in the CA3 cell layer.[54]

The technique of current source density (CSD) was used to further examine the evoked current source/sink distribution within the tissue as a function of location (x). Because the VACNF array was a line, a 1-D current source density was calculated and plotted with the location of electrode 1 set to the origin (Figure 6F)[55,56]

$$I_x = -\sigma(E_{x-h} - 2E_x + E_{x+h})/4h^2 \tag{3}$$

where I_x is the current at location x, h is the spatial resolution, E_{x-h}, E_x, and E_{x+h} are the extracellular voltages at locations $x - h$, x, and $x + h$, and σ is the conductivity of the extracellular space in the tissue. The extracellular space in hippocampal slices was assumed to be isotropic in the presence of a CSF perfusion, an assumption that does not alter the calculated location or timing of current sinks/sources in the hippocampus.[57] Thus, the general characteristics of the CSD were unaffected by the modification of the conductivity component σ which was set to 1 so that the CSD was expressed in units of mV/mm^2.[58]

Twenty channels (odd electrodes from 1 to 39, 30 μm interelectrode spacing) were chosen for the CSD plot which was generated for a constant current, bipolar, biphasic stimulus of 100 μA applied to electrodes 11 (150 μm from the origin) and 29 (420 μm from the origin). To accurately capture the CSD distribution, the electrode spacing must be closer than the size of sinks/sources or smaller than half the spatial wavelength of the tissue activity. Estimates of optimal electrode spacing range from 50 to 100 μm to capture 99% of the CSD power spectrum.[13,55] Figure 6F depicts the calculated CSD and shows the location of current sources and sinks as a function of time. In response to the stimulus,

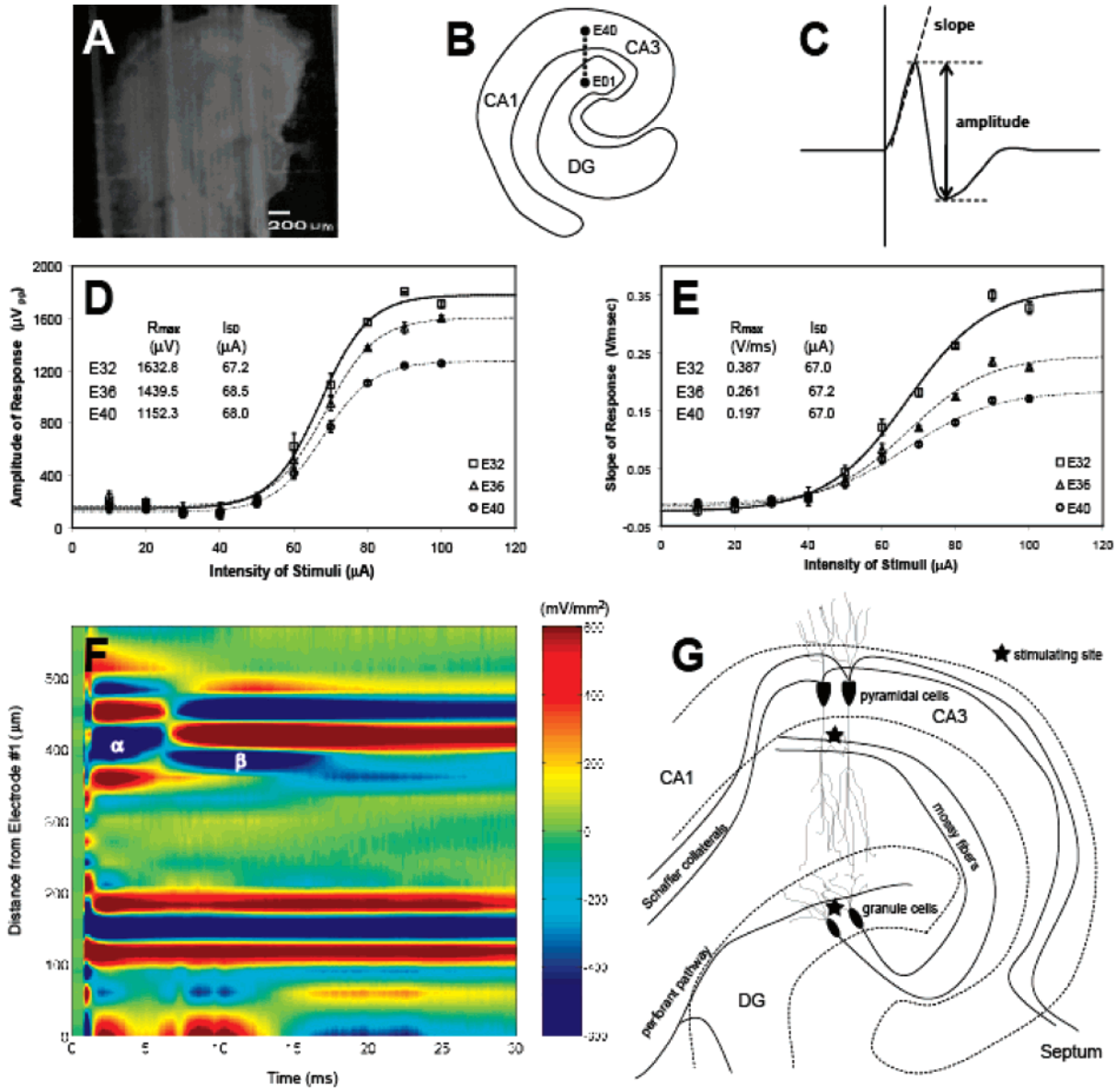

Figure 6. Evoked field potentials recorded by a VACNF array chip were further analyzed. (A) Light micrograph of a hippocampal slice (22 DIV) on a VACNF array chip with the nylon mesh evident. (B) A schematic of the hippocampal anatomy depicting the recording locations. The electrode array crossed the stratum molecular and the stratum radiatum from the DG granule cell layer to the CA3 pyramidal layer. (C) Evoked field potentials recorded from the pyramidal cell layer were analyzed by calculating the slope and peak-to-peak amplitude as shown. The amplitudes of response (D) and slopes (E) of evoked response in three channels (electrodes 32, 36, and 40) were plotted vs intensity of applied stimuli (bipolar, biphasic, constant current from 10 to 100 μA in 10 μA steps, at electrodes 11 and 29; $n = 3$ each). The *S*/*R* curves were fit to a sigmoidal function (eq 2). The net maximum response, R_{max}, was dependent on the distance from the stimulation site, whereas the current that elicited a half-maximal response (I_{50}) was not. The parameter R_0 in (D) and (E) was not zero due to the presence of stimulus artifacts. (F) One-dimension current source density (CSD) was calculated and plotted for 20 channels (odd electrodes from 1 to 39), in response to a constant current, bipolar, biphasic stimulus of 100 μA applied to electrodes 11 and 29; the location of electrode 1 was set to the origin. The α and β denoted different current sinks in the CSD plot. (G) A schematic of the corresponding hippocampal neural circuits helps inform one interpretation of the CSD analysis (F). The first current dipole at α may correspond to activation of the CA3 pyramidal cells whereas the second at β may correspond to mossy fiber depolarization.

the tissue generated a current dipole as neurons began to fire a few milliseconds after stimulation (highlighted by the α in Figure 6F). The current dipole reverses at approximately 7 ms after the stimulus (highlighted by the β in Figure 6F). A 1-D CSD cannot detect currents in the orthogonal direction which complicates its interpretation in the current setting. However, 1-D CSD analysis can still provide insights into functional neuronal circuitry when interpreted in light of the underlying tissue structure.[59,60]

A schematic of the corresponding neural circuits in Figure 6G helps to suggest one possible interpretation of Figure 6F. The first current dipole (α) may correspond to depolarization of the CA3 pyramidal cells whereas the second (β) may correspond to activation of the mossy fibers as they course through the hippocampus. A CSD analysis with a 2-D matrix of VACNF electrodes would better capture the 2-D distribution of electrical activity in the hippocampal slice, whereby stronger inferences of the functional neural connectivity could

be made, as previously reported for the asymmetric distribution of Schaffer projections in CA1.[61,62]

Discussion. Our understanding of distributed neuronal network processing has been facilitated by the advent of MEA recording platforms.[1,2] Simultaneous recording from multiple locations within a tissue may unlock the neural code underlying higher brain functions.[2] We have introduced a new type of MEA with electrodes made not of metal but of vertically aligned carbon nanofibers. We have shown here that these arrays can perform the standard complement of electrophysiological techniques possible with commercial MEAs. The potential benefits afforded by VACNF electrodes are briefly discussed below.

Although the VACNF electrode dimensions are on the submicrometer scale, their noise level is low and comparable to other MEAs.[25] Spontaneous activity was readily discernible above this noise floor. The VACNF electrodes also successfully stimulated the tissue indicating that, despite their small size, the CNF materials has a sufficient charge injection capacity to stimulate the tissue. With a maximal stimulus of 100 μA for 100 μs, the VACNF electrodes were able to pass 10 nC of charge without apparent damage to the tissue as evidence by its stable responses, or to the electrodes as evidence by poststimulation imaging. Given the average effective electrode diameter of 4 μm determined from the reduction current in ruthenium hexamine trichloride, the VACNF electrodes have a theoretical maximum charge injection limit of 8 mC/cm^2, which is comparable to iridium oxide and recently reported carbon nanotube electrodes.[63]

When recordings are made from either acute or cultured brain slices, planar MEAs are not ideal because the electrodes are located some distance from the source of electrophysiological signals.[13,24,25,29] The recorded signal at the surface of the slice is attenuated from that achievable with penetrating glass microelectrodes. Additionally, the theoretical spatial resolution of CSD analysis is reduced by the distance between the electrodes and the source, which spatially blurs the recorded signal.[13] The resolution is set not by the density of the recording sites but by the distance to the signal source.[13,61] MEAs with 3-D electrodes overcome these limitations by penetrating through the surface layer estimated to be about 50 μm thick.[23] Compared to planar arrays, spontaneous single unit amplitudes were approximately doubled as were evoked response amplitudes when recorded with the Ayanda arrays.[24,25] Half-maximal stimulus intensity was also reduced by approximately 25%.[25] Although our current VACNF electrodes are 10 μm in length, even this degree of penetration should boost signal and increase the CSD resolution; efforts are underway to increase their length.

The development of new materials and fabrication processes are critical first steps in the development of new devices with increased functionality and applications. Previously, carbon nanotubes[34,64] have demonstrated the necessary electrochemical properties for neuronal interfacing and even stimulation of dissociated hippocampal cells;[63] however, they have not been used to record electrophysiological activity, as shown herein. With this successful demonstration, it is appropriate to highlight the potential advantages of CNF electrodes including (1) improved biocompatibility due to their covalent carbon structure,[32] (2) excellent electrochemical properties and inertness,[33,65] (3) reduced tissue response due to electrode size and geometry,[30] (4) functionalization with specific proteins to improve neuronal interfacing,[66,67] and (5) direct neurochemical sensing through amperometry or cyclic voltammetry.[68−72] We have previously demonstrated the feasibility of measuring concentrations of dopamine, norepinephrine, and 5-hydroxytyramide with VACNF arrays.[50] Additionally, carbon-based electrodes may be functionalized with enzymes to provide analyte specificity to other less easily oxidized species, including glutamate.[73] We believe that VACNF arrays will significantly impact the fields of electrophysiology and neuroscience by enabling multimode recordings (electrical and neurotransmitter) at high spatial resolution.

Acknowledgment. The authors thank Teri Subich, Dale Hensley, Darrell Thomas, and Ben Fletcher for assistance with electrode fabrication. This study was supported in part by Grant 1R21NS052794 (NINDS) to B.M.III and in part by R01EB006316 (NIBIB), by the Material Sciences and Engineering Division Program of the DOE Office of Science (DE-AC05-00OR22725) with UT-Battelle, LLC, and through the Laboratory Directed Research and Development funding program of the Oak Ridge National Laboratory, which is managed for the U.S. Department of Energy by UT-Battelle, LLC. A.V.M. and M.L.S. acknowledge support from the Material Sciences and Engineering Division Program of the DOE Office of Science. A portion of this research was conducted at the Center for Nanophase Materials Sciences, which is sponsored at Oak Ridge National Laboratory by the Division of Scientific User Facilities (DOE).

Note Added after ASAP Publication. This paper was published ASAP on June 30, 2007. A label in Figure 6F was changed. The updated paper was reposted on July 10, 2007.

References

(1) Pine, J. In *Advances in Network Electrophysiology*; Taketani, M., Baudry, M., Eds.; Springer Science+Business Media: New York, 2006; pp 3−23.
(2) Potter, S. M. *Prog. Brain Res.* **2001**, *130*, 49−62.
(3) Thomas, C. A., Jr.; Springer, P. A.; Loeb, G. E.; Berwald-Netter, Y.; Okun, L. M. *Exp. Cell Res.* **1972**, *74*, 61−66.
(4) Marrese, C. A. *Anal. Chem.* **1987**, *59*, 217−218.
(5) Gesteland, R. C.; Howland, B.; Lettvin, J. Y.; Pitts, W. H. *Proc. IRE* **1959**, *47*, 1856−1862.
(6) Robinson, D. A. *Proc. IEEE* **1968**, *56*, 1065−1071.
(7) Gross, G. W.; Rieske, E.; Kreutzberg, G. W.; Meyer, A. *Neurosci. Lett.* **1977**, *6*, 101−105.
(8) Gross, G. W. *IEEE Trans. Biomed. Eng.* **1979**, *26*, 273−279.
(9) Pine, J. *J. Neurosci. Methods* **1980**, *2*, 19−31.
(10) Gross, G. W.; Williams, A. N.; Lucas, J. H. *J. Neurosci. Methods* **1982**, *5*, 13−22.
(11) Novak, J. L.; Wheeler, B. C. *IEEE Trans. Biomed. Eng.* **1986**, *33*, 196−202.
(12) Novak, J. L.; Wheeler, B. C. *J. Neurosci. Methods* **1988**, *23*, 149−59.
(13) Wheeler, B. C.; Novak, J. L. *IEEE Trans. Biomed. Eng.* **1986**, *33*, 1204−1212.
(14) Gross, G. W.; Wen, W. Y.; Lin, J. W. *J. Neurosci. Methods* **1985**, *15*, 243−252.
(15) Gross, G. W.; Rhoades, B. K.; Reust, D. L.; Schwalm, F. U. *J. Neurosci. Methods* **1993**, *50*, 131−143.

(16) Regehr, W. G.; Pine, J.; Cohan, C. S.; Mischke, M. D.; Tank, D. W. *J. Neurosci. Methods* **1989**, *30*, 91−106.
(17) Thiebaud, P.; de Rooij, N. F.; Koudelka-Hep, M.; Stoppini, L. *IEEE Trans. Biomed. Eng.* **1997**, *44*, 1159−1163.
(18) Hakkoum, D.; Muller, D.; Stoppini, L. In *Advances in Network Electrophysiology*; Taketani, M., Baudry, M., Eds.; Springer Science+Business Media: New York, 2006; pp 112−126.
(19) Gholmieh, G.; Soussou, W.; Han, M.; Ahuja, A.; Hsiao, M. C.; Song, D.; Tanguay, A. R., Jr.; Berger, T. W. *J. Neurosci. Methods* **2006**, *152*, 116−129.
(20) Hutzler, M.; Lambacher, A.; Eversmann, B.; Jenkner, M.; Thewes, R.; Fromherz, P. *J. Neurophysiol.* **2006**, *96*, 1638−1645.
(21) Smith, S. L.; Judy, J. W.; Otis, T. S. *J. Neurosci. Methods* **2004**, *133*, 109−114.
(22) Patolsky, F.; Timko, B. P.; Yu, G.; Fang, Y.; Greytak, A. B.; Zheng, G.; Lieber, C. M. *Science* **2006**, *313*, 1100−1104.
(23) Teyler, T. J. *Brain Res. Bull.* **1980**, *5*, 391−403.
(24) Heuschkel, M. O.; Fejtl, M.; Raggenbass, M.; Bertrand, D.; Renaud, P. *J. Neurosci. Methods* **2002**, *114*, 135−148.
(25) Heuschkel, M. O.; Wirth, C.; Steidl, E.; Buisson, B. In *Advances in Network Electrophysiology*; Taketani, M., Baudry, M., Eds.; Springer Science+Business Media: New York, 2006; pp 69−111.
(26) Nam, Y.; Wheeler, B. C.; Heuschkel, M. O. *J. Neurosci. Methods* **2006**, *155*, 296−299.
(27) Jahnsen, H.; Kristensen, B. W.; Thiebaud, P.; Noraberg, J.; Jakobsen, B.; Bove, M.; Martinoia, S.; Koudelka-Hep, M.; Grattarola, M.; Zimmer, J. *Methods* **1999**, *18*, 160−172.
(28) Kristensen, B. W.; Noraberg, J.; Thiebaud, P.; Koudelka-Hep, M.; Zimmer, J. *Brain Res.* **2001**, *896*, 1−17.
(29) Thiebaud, P.; Beuret, C.; Koudelka-Hep, M.; Bove, M.; Martinoia, S.; Grattarola, M.; Jahnsen, H.; Rebaudo, R.; Balestrino, M.; Zimmer, J.; Dupont, Y. *Biosens. Bioelectron.* **1999**, *14*, 61−65.
(30) Peters, J. L.; Miner, L. H.; Michael, A. C.; Sesack, S. R. *J. Neurosci. Methods* **2004**, *137*, 9−23.
(31) Webster, T. J.; Waid, M. C.; McKenzie, J. L.; Price, R. L.; Ejiofor, J. U. *Nanotechnology* **2004**, *15*, 48−54.
(32) Adams, D.; Williams, D. F.; Hill, J. *J. Biomed. Mater. Res.* **1978**, *12*, 35−42.
(33) Thostensona, E. T.; Renb, Z.; Chou, T. W. *Compos. Sci. Technol.* **2001**, *61*, 1899−1912.
(34) Li, J.; Cassell, A.; Delzeit, L.; Han, J.; Meyyappan, M. *J. Phys. Chem. B* **2002**, *106*, 9299−9305.
(35) Merkulov, V. I.; Lowndes, D. H.; Wei, Y. Y.; Eres, G.; Voelkl, E. *Appl. Phys. Lett.* **2000**, *76*, 3555−3557.
(36) Merkulov, V. I.; Melechko, A. V.; Guillorn, M. A.; Simpson, M. L.; Lowndes, D. H.; Whealton, J. H.; Raridon, R. J. *Appl. Phys. Lett.* **2002**, *80*, 4816−4818.
(37) Merkulov, V. I.; Hensley, D. K.; Melechko, A. V.; Guillorn, M. A.; Lowndes, D. H.; Simpson, M. L. *J. Phys. Chem. B* **2002**, *106*, 10570−10577.
(38) Merkulov, V. I.; Melechko, A. V.; Guillorn, M. A.; Lowndes, D. H.; Simpson, M. L. *Appl. Phys. Lett.* **2002**, *80*, 476−478.
(39) Merkulov, V. I.; Melechko, A. V.; Guillorn, M. A.; Lowndes, D. H.; Simpson, M. L. *Chem. Phys. Lett.* **2001**, *350*, 381−385.
(40) Merkulov, V. I.; Guillorn, M. A.; Lowndes, D. H.; Simpson, M. L.; Voelkl, E. *Appl. Phys. Lett.* **2001**, *79*, 1178−1180.
(41) Merkulov, V. I.; Melechko, A. V.; Guillorn, M. A.; Lowndes, D. H.; Simpson, M. L. *Appl. Phys. Lett.* **2001**, *79*, 2970−2972.
(42) Merkulov, V. I.; Lowndes, D. H.; Baylor, L. R. *J. Appl. Phys.* **2001**, *89*, 1933−1937.
(43) Melechko, A. V.; Merkulov, V. I.; Lowndes, D. H.; Guillorn, M. A.; Simpson, M. L. *Chem. Phys. Lett.* **2002**, *356*, 527−533.
(44) Melechko, A. V.; McKnight, T. E.; Hensley, D. K.; Guillorn, M. A.; Borisevich, A. Y.; Merkulov, V. I.; Lowndes, D. H.; Simpson, M. L. *Nanotechnology* **2003**, *14*, 1029−35.
(45) McKnight, T. E.; Melechko, A. V.; Guillorn, M. A.; Merkulov, V. I.; Doktycz, M. J.; Culbertson, C. T.; Jacobson, S. C.; Lowndes, D. H.; Simpson, M. L. *J. Phys. Chem. B* **2003**, *107*, 10722−10728.
(46) Guillorn, M. A.; McKnight, T. E.; Melechko, A.; Merkulov, V. I.; Britt, P. F.; Austin, D. W.; Lowndes, D. H.; Simpson, M. L. *J. Appl. Phys.* **2002**, *91*, 3824−3828.
(47) McKnight, T. E.; Melechko, A. V.; Austin, D. W.; Sims, T.; Guillorn, M. A.; Simpson, M. L. *J. Phys. Chem. B* **2004**, *108*, 7115−7125.
(48) Fletcher, B. L.; McKnight, T. E.; Melechko, A. V.; Hensley, D. K.; Thomas, D. K.; Ericson, M. N.; Simpson, M. L. *Adv. Mater.* **2006**, *18*, 1689−1694.
(49) Melechko, A. V.; Merkulov, V. I.; McKnight, T. E.; Guillorn, M. A.; Klein, K. L.; Lowndes, D. H.; Simpson, M. L. *J. Appl. Phys.* **2005**, *97*.
(50) McKnight, T. E.; Melechko, A. V.; Fletcher, B. L.; Jones, S. W.; Hensley, D. K.; Peckys, D. B.; Griffin, G. D.; Simpson, M. L.; Ericson, M. N. *J. Phys. Chem. B* **2006**, *110*, 15317−15327.
(51) McKnight, T. E.; Melechko, A. V.; Hensley, D. K.; Mann, D. G. J.; Griffin, G. D.; Simpson, M. L. *Nano Lett.* **2004**, *4*, 1213−1219.
(52) Morrison, B., III; Pringle, A. K.; McManus, T.; Ellard, J.; Bradley, M.; Signorelli, F.; Iannotti, F.; Sundstrom, L. E. *Br. J. Pharmacol.* **2002**, *137*, 1255−1268.
(53) Stoppini, L.; Buchs, P.-A.; Muller, D. *J. Neurosci. Methods* **1991**, *37*, 173−182.
(54) Kerkut, G. A.; Wheal, H. W. *Electrophysiology of isolated mammalian CNS preparations*; Academic Press: London, 1981.
(55) Freeman, J. A.; Nicholson, C. *J. Neurophysiol.* **1975**, *38*, 369−382.
(56) Taube, J. S.; Schwartzkroin, P. A. *J. Neurosci.* **1988**, *8*, 1645−1655.
(57) Holsheimer, J. *Exp. Brain Res.* **1987**, *67*, 402−410.
(58) Yeckel, M. F.; Berger, T. W. *J. Neurosci.* **1998**, *18*, 438−450.
(59) Schroeder, C. E.; Mehta, A. D.; Givre, S. J. *Cereb. Cortex* **1998**, *8*, 575−592.
(60) Lakatos, P.; Chen, C. M.; O'Connell, M. N.; Mills, A.; Schroeder, C. E. *Neuron* **2007**, *53*, 279−292.
(61) Shimono, K.; Brucher, F.; Granger, R.; Lynch, G.; Taketani, M. *J. Neurosci.* **2000**, *20*, 8462−8473.
(62) Shimono, K.; Kubota, D.; Brucher, F.; Taketani, M.; Lynch, G. *Brain Res.* **2002**, *950*, 279−287.
(63) Wang, K.; Fishman, H. A.; Dai, H.; Harris, J. S. *Nano Lett.* **2006**, *6*, 2043−2048.
(64) Li, J.; Stevens, R.; Delzeit, L.; Ng, H. T.; Cassell, A.; Han, J.; Meyyappan, M. *Appl. Phys. Lett.* **2002**, *81*, 910−912.
(65) Chauhan, N. B.; Figlewicz, H. M.; Khan, T. *Int. J. Dev. Neurosci.* **1999**, *17*, 255−264.
(66) Fletcher, B. L.; McKnight, T. E.; Melechko, A. V.; Simpson, M. L.; Doktycz, M. J. *Nanotechnology* **2006**, *17*, 2032−2039.
(67) McKnight, T. E.; Peeraphatdit, C.; Jones, S. W.; Fowlkes, J. D.; Fletcher, B. L.; Klein, K. L.; Melechko, A. V.; Doktycz, M. J.; Simpson, M. L. *Chem. Mater.* **2006**, *18*, 3203−3211.
(68) Pantano, P.; Kuhr, W. G. *Anal. Chem.* **1993**, *65*, 623−630.
(69) Oldenziel, W. H.; Westerink, B. H. *Anal. Chem.* **2005**, *77*, 5520−5528.
(70) Pennington, J. M.; Millar, J.; Jones, C. P. L.; Owesson, C. A.; McLaughlin, D. P.; Stamford, J. A. *J. Neurosci. Methods* **2004**, *140*, 5−13.
(71) Stamford, J. A.; Palij, P.; Davidson, C.; Jorm, C. M.; Millar, J. *J. Neurosci. Methods* **1993**, *50*, 279−290.
(72) Johnson, M. D.; Franklin, R. K.; Scott, K. A.; Brown, R. B.; Kipke, D. R. *Proc. IEEE. Eng. Med. Biol. Conf.* **2005**, *27*, 7325−7328.
(73) Boo, H.; Jeong, R. A.; Park, S.; Kim, K. S.; An, K. H.; Lee, Y. H.; Han, J. H.; Kim, H. C.; Chung, T. D. *Anal. Chem.* **2006**, *78*, 617−620.

NL070291A